The structure of cardiac troponin C regulatory domain with bound Cd^{2+} reveals a closed conformation and unique ion coordination

Xiaolu Linda Zhang, Glen F. Tibbits and Mark Paetzel*

Department of Molecular Biology and Biochemistry, Simon Fraser University, South Science Building, 8888 University Drive, Burnaby, British Columbia V5A 1S6, Canada

Correspondence e-mail: mpaetzel@sfu.ca

The amino-terminal domain of cardiac troponin C (cNTnC) is an essential Ca^{2+} sensor found in cardiomyocytes. It undergoes a conformational change upon Ca^{2+} binding and transduces the signal to the rest of the troponin complex to initiate cardiac muscle contraction. Two classical EF-hand motifs (EF1 and EF2) are present in cNTnC. Under physiological conditions, only EF2 binds Ca^{2+}; EF1 is a vestigial site that has lost its function in binding Ca^{2+} owing to amino-acid sequence changes during evolution. Proteins with EF-hand motifs are capable of binding divalent cations other than calcium. Here, the crystal structure of wild-type (WT) human cNTnC in complex with Cd^{2+} is presented. The structure of Cd^{2+}-bound cNTnC with the disease-related mutation L29Q, as well as a structure with the residue differences D2N, V28I, L29Q and G30D (NIQD), which have been shown to have functional importance in Ca^{2+} sensing at lower temperatures in ectothermic species, have also been determined. The structures resemble the overall conformation of NMR structures of Ca^{2+}-bound cNTnC, but differ significantly from a previous crystal structure of Cd^{2+}-bound cNTnC in complex with deoxycholic acid. The subtle structural changes observed in the region near the mutations may play a role in the increased Ca^{2+} affinity. The 1.4 Å resolution WT cNTnC structure, which is the highest resolution structure yet obtained for cardiac troponin C, reveals a Cd^{2+} ion coordinated in the canonical pentagonal bipyramidal geometry in EF2 despite three residues in the loop being disordered. A Cd^{2+} ion found in the vestigial ion-binding site of EF1 is coordinated in a noncanonical 'distorted' octahedral geometry. A comparison of the ion coordination observed within EF-hand-containing proteins for which structures have been solved in the presence of Cd^{2+} is presented. A refolded WT cNTnC structure is also presented.

1. Introduction

Cardiac troponin C (cTnC) is the regulatory subunit in the heterotrimeric troponin complex comprised of troponin C (TnC), troponin I (TnI) and troponin T (TnT). The troponin complex sits on the thin filaments at periodic intervals of seven actin residues (Farah & Reinach, 1995). The cTnC protein senses the cytosolic Ca^{2+} concentration by binding the ion within its N-terminal regulatory domain (cNTnC); this induces a conformational change that partially 'opens up' and exposes its central hydrophobic cavity. This conformational change in cTnC allows the 'switch' region of cTnI (residues 147–163) to bind to it and consequently causes the detachment of the inhibitory region of TnI (residues 128–146) from actin. This

detachment results in exposure of the myosin-binding site on actin, which allows cross-bridging between myosin and actin, leading to muscle contraction (Li *et al.*, 1999; Gordon *et al.*, 2000).

The cNTnC domain contains two EF-hand motifs (EF1 and EF2). The EF hand is a common functional motif that is found in many Ca^{2+}-binding proteins. It consists of a 12-residue ion-binding loop flanked by two perpendicularly positioned α-helices (Kretsinger & Nockolds, 1973). Canonically, the residues at loop positions 1, 3, 5, 7 and 12 participate in coordinating Ca^{2+} (Fig. 1*a*) and the coordinating ligands are positioned in a pentagonal bipyramidal geometry (Fig. 1*b*) (Strynadka & James, 1989). The equatorial plane is constructed from ligands at positions Y, Z, $-Y$ and $-Z$. The $-Z$ position is normally a glutamate residue that contributes its two carboxylate O atoms as a bidentate ligand. The ligands orientated at the X and $-X$ positions make up the vertical axis (Fig. 1*b*). The ligand at the $-X$ position is often a water molecule.

Only one of the two EF hands in cNTnC binds Ca^{2+} under physiological conditions (Li *et al.*, 1997; van Eerd & Takahashi, 1975). By comparing the EF1 loop sequence with canonical EF-hand loop sequences, it can be seen that the residues at positions 1 and 3 are replaced by two nonpolar residues that are unable to coordinate Ca^{2+} ions (van Eerd & Takahashi, 1975). EF2 then serves as the sole Ca^{2+}-binding site in cNTnC at physiological Ca^{2+} concentrations and acts as the lone Ca^{2+} sensor in the troponin complex for cardiac muscle function (Li *et al.*, 1997). This is supported by NMR studies of Ca^{2+}-bound human cNTnC, which show that Ca^{2+} is only observed in EF2 (Spyracopoulos *et al.*, 1997). To reveal the atomic details of ion coordination within the EF hands of the protein, a high-resolution crystal structure of cNTnC is needed.

A Leu29-to-glutamine (L29Q) mutation in cardiac troponin C was found in a human patient with hypertrophic cardio-

myopathy (HCM; Hoffmann *et al.*, 2001), which is a leading cause of sudden cardiac death in young people and athletes. Its prevalence is about 1 in 500 in the general population (Wang *et al.*, 2010). Interestingly, in an evolutionary study of cardiac troponin C by Gillis *et al.* (2007), ectothermic species (for example, rainbow trout) were found to have a glutamine at position 29, as well as three other conserved residue differences from human cTnC (D2N, V28I and G30D). These four residues, Asn2, Ile28, Gln29 and Asp30 (NIQD), have functional importance in Ca^{2+} sensing at lower temperatures (the physiological temperature of most ectothermic species living in temperate climates; Gillis *et al.*, 2007). This has been supported by observations of a higher Ca^{2+} affinity for the NIQD mutant of human cTnC (Gillis *et al.*, 2005). Spyracopoulos and coworkers also suggested previously that the EF1 and EF2 loops are structurally linked (Spyracopoulos *et al.*, 1997). Therefore, primary sequence differences in site I may have an effect on the structure and thus the ion-binding ability of site II (Gillis *et al.*, 2007). Determination of the L29Q and NIQD cNTnC structures may provide greater insight into conformational changes and their ramifications.

Although the structure of the human cNTnC domain has been studied extensively by NMR (Spyracopoulos *et al.*, 1997; Li *et al.*, 1999; Robertson *et al.*, 2010; Wang *et al.*, 2002), few crystal structures of cNTnC are available owing to difficulty in forming ordered crystals. We have recently found that the presence of Cd^{2+} in the crystallization conditions results in cNTnC crystals that diffract to high resolution (Li *et al.*, 2011). Cd^{2+} is similar to Ca^{2+} in terms of ionic radius (Cd^{2+}, 0.97 Å; Ca^{2+}, 0.99 Å). Therefore, it is able to replace Ca^{2+} ions in many Ca^{2+}-binding proteins without disrupting the protein structure (Rao *et al.*, 1996). An isotope of cadmium, ^{113}Cd, is often used in NMR analysis of Ca^{2+}-binding proteins (Forsén *et al.*, 1979).

Here, we present a 1.4 Å resolution crystal structure of WT human cNTnC that coordinates Cd^{2+} in both the EF1 and EF2 loops, including the EF1 vestigial site. The structure has a similar overall conformation to that observed in Ca^{2+}-bound NMR structures (Spyracopoulos *et al.*, 1997), but differs significantly from our previous crystal structure of Cd^{2+}-bound cNTnC in complex with deoxycholic acid (Li *et al.*, 2011). Analysis of the ion coordination in both EF1 and EF2 reveals differences from what has previously been observed in cTnC. In EF2, while Cd^{2+} is coordinated in a canonical pentagonal bipyramidal geometry, the binding loop is partially disordered, with two of the coordinating residues [Asp67 (Y) and Ser69 (Z)] being replaced by water molecules. A Cd^{2+} ion bound within EF1 (the normally empty vestigial site) shows a noncanonical 'distorted' octahedral geometry.

Structures of L29Q cNTnC at 1.9 Å resolution and NIQD cNTnC at 2.0 Å resolution were also determined. In both structures, the mutations caused local main-chain shifts within the EF1 loop, but did not cause overall conformational changes or changes within the EF2 loop in cNTnC compared with the WT counterpart.

A 1.6 Å resolution refolded cNTnC structure is also presented here to depict the effect of refolding on the structure of cNTnC.
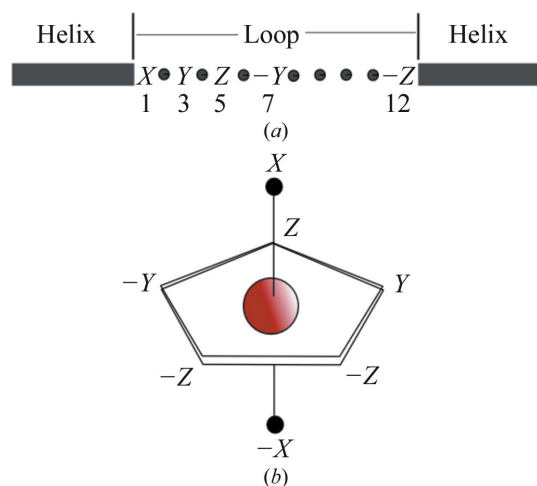

Figure 1
Canonical pentagonal bipyramidal geometry coordination displayed by EF-hand ion-binding proteins. (*a*) Flanked by two helices, the EF-hand ion-coordinating loop contains 12 residues. The residues at positions 1, 3, 5, 7 and 12 are labelled with their spatial orientation in pentagonal bipyramidal geometry. (*b*) Spatial orientation of coordinating ligands in canonical pentagonal bipyramidal geometry.

Table 1
Data-collection and refinement statistics.

Values in parentheses are for the outer shell.

	High resolution	SAD	Refolded WT	L29Q	NIQD
PDB code	3sd6	3swb	4gje	4gjf	4gjg
Beamline	CLS 08ID-1	NSLS X4A	CLS 08B1-1	CLS 08ID-1	CLS 08ID-1
Crystal parameters					
Space group	$P6_122$	$P6_122$	$P6_122$	$P6_122$	$P6_122$
Unit-cell parameters (Å)					
$a = b$	49.6	49.8	49.6	49.3	49.6
c	116.0	117.4	116.3	113.4	115.1
Matthews coefficient ($Å^3 Da^{-1}$)	2.11	2.15	2.06	1.98	2.02
Solvent content (%)	41.72	42.94	40.45	37.87	39.21
Data-collection statistics					
Wavelength (Å)	0.97949	0.97910	0.97921	0.97949	0.97949
Resolution (Å)	42.93–1.37	43.12–1.67	42.98–1.60	42.66–1.90	42.91–2.00
	(1.42–1.37)	(1.73–1.67)	(1.66–1.60)	(1.97–1.90)	(2.07–2.00)
Total reflections	190197	383749	242530	66732	57016
Unique reflections	17420 (1251)	10488 (982)	11912 (1155)	6990 (662)	6190 (594)
R_{merge}	0.050 (0.442)	0.128 (0.432)	0.058 (0.382)	0.062 (0.327)	0.091 (0.409)
Mean $I/\sigma(I)$	64.07 (2.283)	102.75 (11.632)	84.85 (11.967)	55.09 (8.650)	46.91 (8.441)
Completeness (%)	97.0 (79.8)	99.9 (99.9)	99.9 (100.0)	99.7 (99.8)	99.8 (100.0)
Multiplicity	10.5 (4.3)	35.8 (17.8)	20.4 (20.6)	9.5 (9.8)	9.2 (9.1)
Phasing statistics					
No. of Cd sites	—	5	—	—	—
FOM	—	0.713	—	—	—
Refinement statistics					
Protein molecules in asymmetric unit	1	1	1	1	1
Residues	86	86	86	86	86
Waters	49	45	67	45	34
Cadmiums	7	6	7	8	7
Calciums	2	3	2	1	3
Acetates	2	1	3	1	1
Glycerols	—	—	—	1	1
Total No. of atoms	745	738	766	742	731
R_{cryst}/R_{free} (%)	13.5/14.8	13.5/16.5	12.1/15.0	14.2/17.8	14.4/19.8
Average B factors ($Å^2$)					
All atoms	25.6	24.7	28.3	40.5	38.7
Protein	25.3	24.1	26.8	38.8	37.2
Waters	38.6	36.2	43.5	63.6	62.4
Cadmiums	19.6	19.5	22.2	35.4	39.7
Calciums	28.8	27.0	27.9	175.4	76.8
Acetate ions	29.5	27.7	35.1	36.9	41.7
Glycerols	—	—	—	50.6	50.2
R.m.s.d. on angles (°)	1.833	1.908	1.735	1.640	1.585
R.m.s.d. on bonds (Å)	0.018	0.018	0.018	0.016	0.015
Ramachandran plot statistics, No. of residues in					
Preferred regions	80 [97.56%]	80 [97.56%]	80 [97.56%]	80 [97.56%]	81 [98.78%]
Allowed regions	2 [2.44%]	2 [2.44%]	2 [2.44%]	2 [2.44%]	1 [1.22%]
Outliers	0 [0.00%]	0 [0.00%]	0 [0.00%]	0 [0.00%]	0 [0.00%]
Residues missing owing to lack of electron density	3 [67–69]	3 [67–69]	3 [67–69]	3 [67–69]	3 [67–69]

2. Materials and methods

2.1. Overexpression and purification of WT cNTnC

The previously described plasmid pET21a_WT_cNTnC_1-89 (Li *et al.*, 2011) was transformed into *Escherichia coli* expression host BL21 (DE3) competent cells. The expressed protein (cNTnC) is 89 residues in length (residues 1–89 of human troponin C; UniProt accession No. P63316) with a calculated molecular mass of 10 062 Da and a theoretical isoelectric point of 4.0. Cells containing the plasmid were grown at 310 K in LB medium (100 µg ml^{-1} ampicillin) until the OD_{600} reached 0.6. The cells were then induced with isopropyl β-D-1-thiogalactopyranoside (IPTG) at a final concentration of 1 mM and were incubated for an additional 4 h at 310 K. Cell pellets were collected by centrifugation at

6000g for 7 min at 277 K and were resuspended in resuspension buffer [10 mM Tris–HCl pH 8.0, 1 mM dithiothreitol (DTT); three times the volume of the pellet]. The cells were sonicated for 45 s at 30% amplitude using a Model 500 Dismembrator (Fisher Scientific) and lysed using an Avestin EmulsiFlex-C3 high-pressure homogenizer set to 103–138 MPa for 5 min. The lysate was centrifuged at 28 964g for 35 min at 277 K and the supernatant was loaded onto a Q-Sepharose anion-exchange column (5 ml column volume; GE Healthcare) pre-equilibrated with resuspension buffer. After washing the column with 10 ml resuspension buffer, elution was performed in five steps with an increasing NaCl concentration (100–500 mM in 100 mM increments). Samples of the elution fractions were run on a 15% SDS–PAGE gel. Fractions containing cNTnC were combined and concentrated

to a volume of 5 ml using an Amicon centrifugal filter unit (5 kDa cutoff, Millipore). The protein was then further purified using a size-exclusion chromatography column (HiPrep 26/60 Sephacryl S-100 High-Resolution) on an ÄKTAprime system (Pharmacia Biotech). The column was equilibrated with 10 mM Tris–HCl pH 8.0, 150 mM NaCl, 1 mM DTT and run at a flow rate of 1.0 ml min^{-1}. All fractions containing cNTnC were identified using 15% SDS–PAGE and concentrated to 20 mg ml^{-1} using an Amicon centrifugal filter unit (5 kDa cutoff, Millipore). The concentration was determined with a NanoDrop ND-100 spectrophotometer (Thermo Scientific) using an extinction coefficient of 1490 M^{-1} cm^{-1} (ProtParam; Walker, 2005).

2.2. Overexpression and purification of L29Q and NIQD cNTnC

The L29Q and NIQD cNTnC constructs (residues 1–89) were made from full-length L29Q and NIQD cTnC constructs by converting Lys90 to a termination codon by site-directed mutagenesis (SDM). The SDM primers used have been described previously (Li et al., 2011). The overexpression and purification procedures were the same as those described for WT cNTnC.

2.3. Protein refolding

For one of the crystal structures (PDB entry 4gje), the purified WT cNTnC was subjected to refolding before being used for crystallization. The protein was first denatured in buffer consisting of 4 M guanidine–HCl, 10 mM Tris–HCl pH 8.0, 1 mM DTT. It was then dialyzed against buffer consisting of 10 mM Tris–HCl pH 8.0, 1 mM DTT to remove the denaturant. The protein remained soluble throughout the refolding process.

2.4. Crystallization

The sitting-drop vapour-diffusion method was used to grow the crystals in this study. Each crystallization drop was prepared by mixing 1 µl purified protein solution (20 mg ml^{-1}) with 1 µl reservoir solution and was equilibrated against 1 ml reservoir solution. The reservoir solution used for the crystals that generated the high-resolution WT cNTnC and refolded WT cNTnC data sets consisted of 0.05 M cadmium sulfate octahydrate, 1.0 M sodium acetate, 0.1 M HEPES pH 7.5, while the crystals for the SAD, L29Q and NIQD cNTnC data set were obtained from conditions consisting of 0.02 M cadmium sulfate octahydrate, 0.6 M sodium acetate, 0.1 M Tris–HCl pH 8.0. In both cases crystals grew in 3 d at room temperature (298 K). The crystals were flash-cooled in liquid nitrogen in a 0.2 mm CrystalCap copper magnetic loop (Hampton Research) using a cryoprotectant solution that had the same chemical components as the respective reservoir solution but with glycerol replacing 30% of the water.

2.5. Anomalous data collection

The SAD data set for WT cNTnC was collected on beamline X4A at the National Synchrotron Light Source using a wavelength of 0.97910 Å. The detector was an ADSC Quantum 4r CCD. A total of 720 images were collected with a 0.5° oscillation angle and a 10 s exposure time, while the crystal-to-detector distance was 160 mm. The diffraction images were integrated and scaled with HKL-2000 (Otwinowski & Minor, 1997). Reflections were detectable to 1.7 Å resolution and the Matthews coefficient and solvent content were calculated using the CCP4 suite (Winn et al., 2011). Crystal parameters and data-collection statistics are given in Table 1.

2.6. High-resolution data collection

The high-resolution diffraction data set was collected on beamline 08ID-1 of the Canadian Light Source, Canadian Macromolecular Crystallography Facility using a wavelength of 0.97949 Å. A MAR Mosaic 300 mm CCD detector was used with a crystal-to-detector distance of 180 mm, and a total of 201 images were collected with a 0.5° oscillation angle and a 0.6 s exposure time. The diffraction data were processed with HKL-2000 (Otwinowski & Minor, 1997). Reflections were detectable to 1.4 Å resolution and the Matthews coefficient and solvent content were calculated using the CCP4 suite (Winn et al., 2011). Crystal parameters and data-collection statistics are given in Table 1.

2.7. Refolded WT cNTnC data collection

The refolded WT cNTnC data set was collected on beamline 08B1-1 of the Canadian Light Source, Canadian Macromolecular Crystallography Facility using a wavelength of 0.97921 Å. A Rayonix MX300HE CCD detector was used with a crystal-to-detector distance of 180 mm, and a total of 180 images were collected with a 1° oscillation angle and a 5 s exposure time. The diffraction data were processed using HKL-2000 (Otwinowski & Minor, 1997). Reflections were detectable to 1.5 Å resolution. Crystal parameters and data-collection statistics are given in Table 1.

2.8. L29Q and NIQD cNTnC data collection

The L29Q and NIQD cNTnC data sets were collected on beamline 08ID-1 of the Canadian Light Source, Canadian Macromolecular Crystallography Facility using a wavelength of 0.97949 Å. A MAR Mosaic 300 mm CCD detector was used with a crystal-to-detector distance of 210 mm for L29Q cNTnC. A total of 120 images were collected with a 0.75° oscillation angle and a 1 s exposure time. For NIQD cNTnC, the crystal-to-detector distance was 200 mm and 90 images were collected with a 1° oscillation and a 1 s exposure time. The diffraction data were processed with HKL-2000 (Otwinowski & Minor, 1997). Reflections were detectable to 1.7 Å resolution for L29Q cNTnC and to 1.8 Å resolution for NIQD cNTnC. Crystal parameters and data-collection statistics are given in Table 1.

2.9. SAD phasing and structure solution

The program HKL2MAP (Pape & Schneider, 2004) was used to search for cadmium sites at 2.2 Å resolution, and five

sites with an occupancy higher than 0.5 were found. The electron-density map generated by *HKL2MAP* (Pape & Schneider, 2004) was then used for model building in *PHENIX* (Adams *et al.*, 2010). The final model was optimized by manual building in *Coot* (Emsley & Cowtan, 2004) and rounds of restrained refinement in *REFMAC* v.5.5.0109 (Murshudov *et al.*, 2011). The data-collection and refinement statistics are presented in Table 1. The atomic coordinates and structure factors have been deposited in the Protein Data Bank (PDB entry 3swb).

2.10. Structure determination and refinement of the high-resolution data set

Phases for the high-resolution data set were obtained by molecular replacement using the program *Phaser* (McCoy *et al.*, 2007). The coordinates of the SAD data-set structure were used as a search model. Manual adjustments to the initial model were performed in the program *Coot* (Emsley & Cowtan, 2004) and the structure was refined using restrained refinement in *REFMAC*5 (Murshudov *et al.*, 2011). Seven Cd^{2+} ions and two Ca^{2+} ions were observed in the structure. The two

different types of ions were distinguished by fitting Cd^{2+} or Ca^{2+} into the difference electron-density maps. Because of the significant difference in the number of electrons between these ions, only one of the two ions would fit the electron density without creating positive or negative difference density after refinement. The complete data-collection and refinement statistics are summarized in Table 1. The atomic coordinates and structure factors have been deposited in the Protein Data Bank (PDB entry 3sd6).

2.11. Structure determination and refinement of L29Q, NIQD and refolded WT cNTnC

Phases for these three data sets were obtained by molecular replacement with the program *MOLREP* (Vagin & Teplyakov, 2010) using the coordinates of the high-resolution data-set structure as a search model. Manual adjustments to the initial model were performed using the program *Coot* (Emsley & Cowtan, 2004) and the structure was refined using restrained refinement in *REFMAC*5 (Murshudov *et al.*, 2011). The complete data-collection and refinement statistics are summarized in Table 1. The atomic coordinates and structure factors have been deposited in the Protein Data Bank (PDB entries 4gje for refolded WT cNTnC, 4gjf for L29Q cNTnC and 4gjg for NIQD cNTnC).

2.12. Structural analysis

The root-mean-square deviation (r.m.s.d.) values reported for all-atom protein superpositions were calculated using *PyMOL* (DeLano, 2002) and atomic distances were measured using the program *Coot* (Emsley & Cowtan, 2004). To visualize central hydrophobic cavity exposure, the structures were displayed in inverted surface-cavity mode using *PyMOL* (DeLano, 2002).

2.13. Figure preparation

The structural figures were generated in *PyMOL* (DeLano, 2002).

3. Results and discussion

3.1. Protein structure solution

Human cNTnC (residues 1–89) with the WT primary sequence was successfully expressed, purified and crystallized, and its structure was determined by anomalous diffraction methods. This structure was used as a molecular-replacement search model to obtain phases for a higher resolution data set. The 1.4 Å resolution structure contained one molecule in the asymmetric unit and included 86 of the 89 residues within the protein. Three residues (residues 67–69) were not modelled owing to a lack of electron density. The final refined model has an R_{work} of 13.5% and an R_{free} of 14.8%. Along with the 86 residues from the single protein chain, seven cadmium ions, two calcium ions, two acetate ions and 49 water molecules were modelled. The average B factor of the structure is
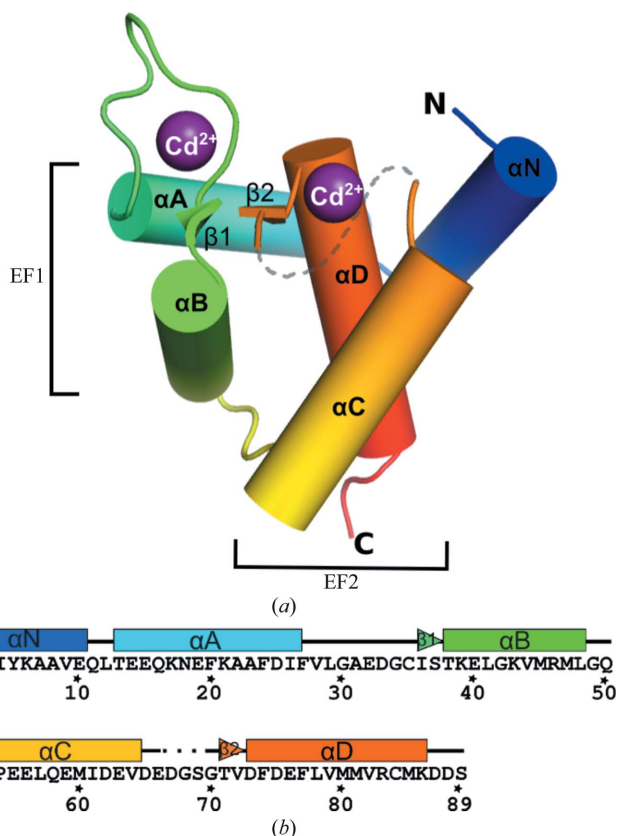
Figure 2
Overall protein fold of Cd^{2+}-bound human cNTnC. (*a*) WT human cNTnC contains five α-helices (αN, αA, αB, αC and αD) and two β-strands (β1 and β2). Two EF-hand motifs are present in the structure: EF1 and EF2. Each EF loop coordinates a Cd^{2+} ion. The three residues missing from the EF2 loop region owing to a lack of electron density are represented by a grey dashed line. (*b*) Secondary structure of Cd^{2+}-bound human cNTnC aligned with the primary sequence (UniProt accession No. P63316). The α-helices and β-strands are presented in the same colour scheme as in (*a*).
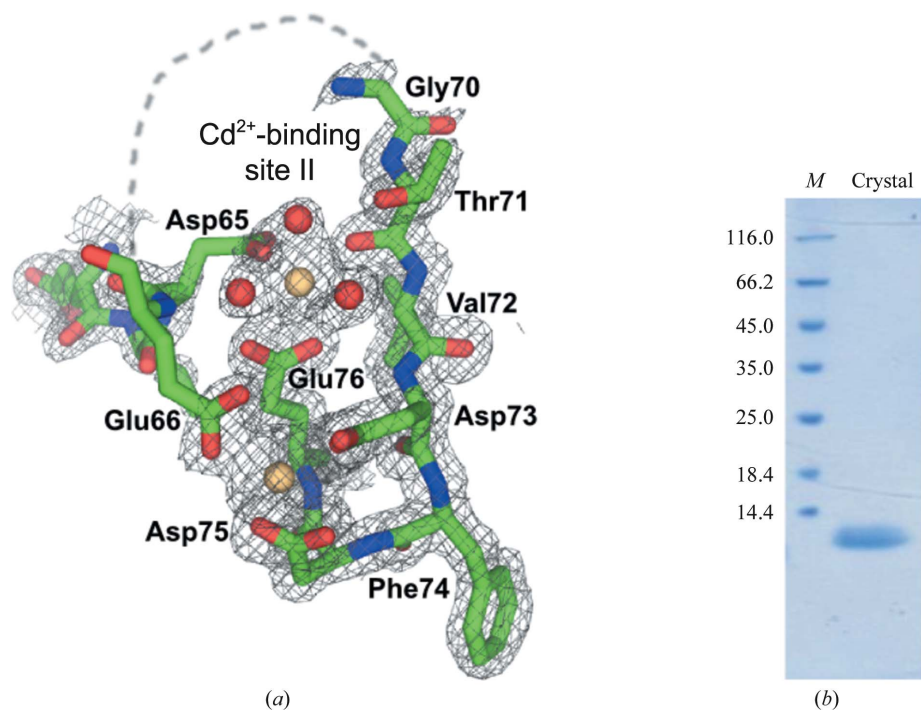
(a)

(b)

Figure 3
Three residues within EF2 are disordered in the Cd^{2+}-bound cNTnC structure. (*a*) Electron density ($2F_o - F_c$, at the 1.0σ level) is shown for the region near the Cd^{2+} bound in EF2. No clear electron density is visible for residues 67, 68 and 69. The missing residues are represented by a dashed line. The cNTnC residues are shown as sticks (carbon, green; nitrogen, blue; oxygen, red; sulfur, yellow). The Cd^{2+} ion and water molecules are represented by light orange and red spheres, respectively. (*b*) An SDS–PAGE gel (stained with PageBlue) of the cNTnC crystal used in data collection shows a single protein band at ~10 kDa. *M* stands for molecular mass standards (in kDa).

25.6 $\mathring{A}^2$. Ramachandran plot statistics indicate that no residue outliers are present in the final model (Table 1).

The L29Q, NIQD and refolded WT cNTnC structures were all determined by molecular replacement using the high-resolution data set as a search model. Refinement statistics for these structures are summarized in Table 1.

3.2. Overall protein fold of WT cNTnC

The WT cNTnC structure contains five α-helices (αN, αA, αB, αC and αD) and two short β-strands (β1 and β2) (Fig. 2*a*). The EF1 motif is comprised of αA (residues 13–27), loop 1 (residues 28–37) and αB (residues 38–48), while the EF2 motif is comprised of αC (residues 53–64), loop 2 (residues 65–72) and αD (residues 73–86) (Fig. 2*b*). A short two-stranded antiparallel β-sheet, sometimes referred as the 'EF β-scaffold' (Grabarek, 2006), formed by β1 (residues 36–37) and β2 (residues 71–72) within EF1 and EF2 brings the two ion-binding loops into close proximity to each other.

Clear and sharp electron density is observed for every residue within the protein chain except for the three residues 67–69, which are within the EF2 loop (Fig. 3*a*). An SDS–PAGE gel of the protein crystal that generated the structure showed a single band at ~10 kDa which corresponds to the approximate molecular mass of cNTnC (Fig. 3*b*). This suggests that the lack of electron density for the three EF2 loop residues is the result of thermal motion rather than the result of

proteolytic cleavage or radiation damage at this site. Investigation of the crystalline lattice shows that this region of the loop faces a solvent channel.

3.3. The L29Q and NIQD mutations cause a subtle main-chain shift in the EF1 loop of cNTnC

The electron-density maps confirmed the mutations in the L29Q and NIQD structures. In Fig. 4(*a*), the L29Q cNTnC data set was refined with a WT leucine at position 29. Positive difference density ($F_o - F_c$, at the 3.0σ level) appears at the end and along the side of the leucine side chain. This suggests that the side chain of residue 29 should be more extended than leucine (*i.e.* with a branching point at C^δ instead of C^γ) and glutamate is a better fit to the density.
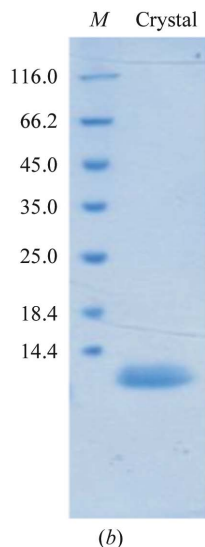
In Fig. 4(*b*), the NIQD cNTnC data set was refined with WT residues: valine at position 28, leucine at position 29 and glycine at position 30. For V28I, positive difference density (at the 3.0σ level) appeared at one of the C^γ ends of valine. This is a clear indication of isoleucine instead of valine. Also, positive difference densities for both L29Q and G30D render distinct shapes for the side chains of the mutated residues Gln29 and Asp30 (Fig. 4*b*). This strongly supports the presence of L29Q and G30D in NIQD cNTnC. Superimposition of WT, L29Q and NIQD cNTnC (Fig. 4*c*) showed no significant overall structural difference among the three structures. The all-atom r.m.s.d. value between L29Q and WT cNTnC is 0.187 Å and that between NIQD and WT cNTnC is 0.123 Å (DeLano, 2002).

L29Q is located at the beginning of the EF1 loop of cNTnC. This mutation of a nonpolar leucine to a polar glutamine extends the side chain of residue 29 by one atom. Its side chain points away from the protein molecule and into the solvent channel between neighbouring protein molecules. The presence of $O^{\varepsilon 1}$ and $N^{\varepsilon 2}$ of Glu29 did not create extra hydrogen bonds at the position of residue 29 in the structure. However, the main chain between residues 29 and 32 shifted towards the solvent channel by up to 0.5 Å in L29Q cNTnC compared with the WT. The presence of the L29Q mutation did not change the Cd^{2+} coordination in EF1 compared with its WT counterpart.

In the NIQD cNTnC mutant, which contains V28I, L29Q and G30D mutations in the EF1 loop, the Cd^{2+} coordination in EF1 is also not altered compared with its WT counterpart. The main chain between residues 29 and 32 is also shifted towards the solvent channel in the NIQD mutant by up to 1.0 Å compared with the WT. The change from glycine at position 30

to aspartic acid introduces a new hydrogen bond between the $O^{\delta 1}$ atom of the Asp30 side chain and the main-chain N atom of Asp30. The two O^{δ} atoms of Asp30 also form hydrogen bonds to three separate water molecules.

It has previously been proposed that since the EF1 and EF2 loops are structurally linked, sequence mutations in the EF1 loop may alter the structure of the EF2 loop in cNTnC and thus may affect the ion-binding ability of EF2 (Spyracopoulos *et al.*, 1997; Gillis *et al.*, 2007). However, superimposition of WT, L29Q and NIQD cNTnC did not show any differences in the EF2 loop among the three structures (Fig. 4c), nor is the coordination of Cd^{2+} in EF2 changed. Therefore, it is likely to be the nonpolar-to-polar mutations (leucine 29 to glutamine and glycine 30 to aspartic acid) that account for the increased Ca^{2+} affinity (Liang *et al.*, 2008) in L29Q and NIQD cNTnC.
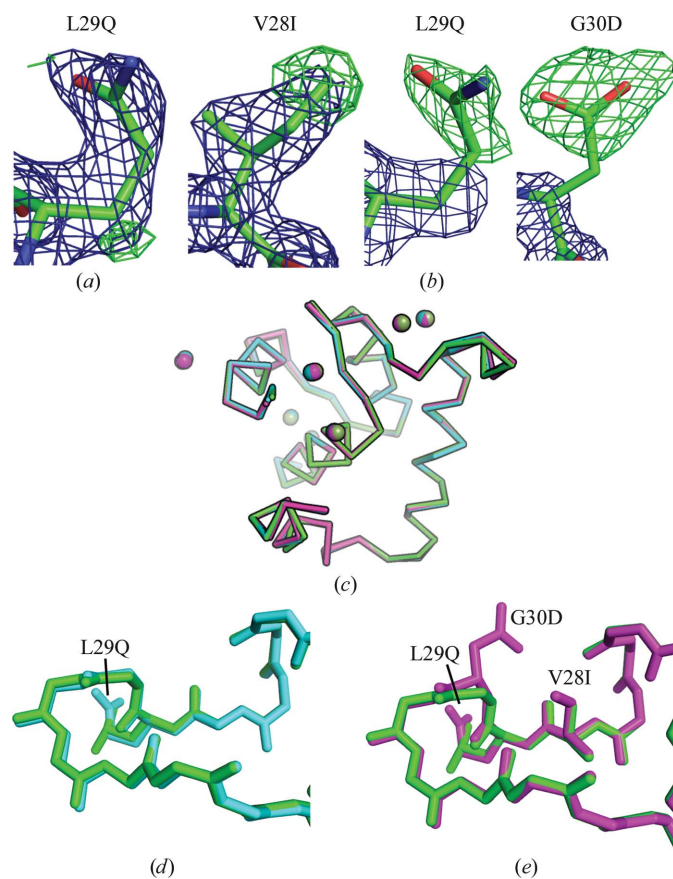

Figure 4
Crystal structures of L29Q and NIQD cNTnC. Electron density ($2F_o - F_c$, at the 1.0σ level, blue mesh) and difference density ($F_o - F_c$, at the 3.0σ level, green mesh) are shown for the region of cNTnC with (a) an L29Q mutation in L29Q cNTnC and (b) V28I, L29Q and D30G mutations in NIQD cNTnC. Each of these figures shows the electron densities when refined with the WT sequence residues (*i.e.* Val28, Leu29 and Gly30). The mutated residues are shown as sticks (carbon, green; nitrogen, blue; oxygen, red). (c) Superimposition of WT (green), L29Q (cyan) and NIQD (magenta) cNTnC (shown as ribbons). The Cd^{2+} ion in each structure is shown as a sphere. Superimposition of (d) L29Q (cyan) and WT (green) cNTnC and (e) NIQD (magenta) and WT cNTnC with a focus on the EF1 loop region. The main-chain shift is visible in both cases. Protein chains are shown as sticks.

As shown in the mutant structures (Figs. 4d and 4e), both residues 29 and 30 are located on the surface of the protein and their side chains face the solvent. Nonpolar-to-polar mutations at these positions tend to increase the surface hydrophilicity of the protein. It has been demonstrated previously that an increase in the surface hydrophilicity of proteins (such as trypsin and subtilisin) results in the proteins being more easily activated (Genicot *et al.*, 1996; Smalås *et al.*, 1994). The increased interaction between the protein and solvent decreases the free energy that needs to be overcome for the conformational change that leads to protein activation to occur (Gillis *et al.*, 2007).

3.4. The overall conformation of Cd^{2+}-bound cNTnC resembles that of Ca^{2+}-bound cNTnC

The overall conformation of our Cd^{2+}-bound cNTnC structure resembles that of the Ca^{2+}-bound structures. An all-atom superimposition of the Cd^{2+}-bound cNTnC crystal structure with a representative chain of the Ca^{2+}-bound cNTnC NMR structure (PDB entry 1ap4; Spyracopoulos *et al.*, 1997) results in an r.m.s.d. of 1.65 Å (Fig. 5a).

The two other available crystal structures of cNTnC adopt a different conformation compared with the structure presented here. The crystal structures of Ca^{2+}-bound human cNTnC with Cys35 mutated to serine and with bound trifluoroperazine (TFP; PDB entry 1wrk; S. Takeda, T. Igarashi, Y. Oishi & H. Mori, unpublished work) superimposes onto our structure with an r.m.s.d. of 2.60 Å. The position of helix B is the major difference between the structures (Fig. 5b), as it moves away from the centre of the molecule. The crystal structure of WT human cNTnC coordinating Cd^{2+} in both EF loops and in complex with deoxycholic acid (DXC; Li *et al.*, 2011) reveals a significantly different conformation to the Cd^{2+}-bound cNTnC in the absence of DXC that is presented here. The A helices in the two structures are oriented approximately 90° apart, and all-atom superposition of the two structures results in an r.m.s.d. of 8.00 Å (Fig. 5c).

Examination of the above three cNTnC crystal structures reveals that there are differences in the degree of 'openness' (Fig. 6). The term 'openness' refers to a measure of how far apart helices A and B are positioned relative to helices C and D. The further apart the two groups of helices are, the more exposed the central hydrophobic core is. Our Cd^{2+}-bound cNTnC represents the most closed (or that with the lowest degree of 'openness') structure among the three. The Cd^{2+}-bound cNTnC in complex with DXC has the highest degree of 'openness'. The three structures are placed on a closed-to-open scale in Fig. 6.

While TFP is a Ca^{2+}-sensitizing drug that increases the Ca^{2+} affinity of troponin C and muscle contractility (Kass & Solaro, 2006; Endoh, 2007), DXC is a derivative of bile acid (Hofmann, 1999). The two chemicals have similar structural characteristics in that they both contain a hydrophobic ring system and a hydrophilic group at the end. The hydrophobicity of the ring system allows these chemical compounds to bind within the central hydrophobic core of cNTnC and

stabilize the open conformation of cNTnC. Fig. 6 shows how TFP and DXC are bound at the hydrophobic core of cNTnC.

Before the structure presented here was determined, it was unclear which contributed more to the observed wide-open conformation: Cd^{2+} binding at the EF loops or the presence of DXC (Li *et al.*, 2011). It is now clear that Cd^{2+} binding to the EF loops of cNTnC does not by itself induce the wide-open conformation. It is likely that the presence of compounds such as DXC and TFP in the hydrophobic core of the protein contributes to the stabilization of the open conformation of cNTnC (Fig. 6). There are examples of other Ca^{2+}-sensitizing drugs that also stabilize the open conformation of cNTnC (Robertson *et al.*, 2010; Wang *et al.*, 2002).

3.5. EF1 coordinates Cd^{2+} in a 'distorted' octahedral geometry

The Cd^{2+} ion located in EF1 is co-ordinated by six ligands (Fig. 7a). The main-chain carbonyl O atom of Cys35 and the oxygen from a water take up the axial positions X and $-X$, respectively. The equatorial plane is constructed by Asp33 $O^{\delta 2}$ (Y), Asp33 $O^{\delta 1}$ (Z), Cys35 S^{γ} ($-Y$) and acetate OXT ($-Z$) (Fig. 7c). This makes the Cd^{2+} coordination at the EF1 loop noncanonical, as the ion is coordinated in a 'distorted' octahedral geometry. This is the first time that this coordination geometry has been observed in an EF loop of cNTnC, but octahedral coordination has been observed in the EF loops of other Ca^{2+}-binding proteins (Gifford *et al.*, 2007; Grabarek, 2011); for example, the Ca^{2+}-binding apoptosis-linked gene-2 (ALG-2) protein (Jia *et al.*, 2001). Ca^{2+} is coordinated in an octahedral geometry using only residues from the N-terminal half of the EF loop. The octahedral coordination is also utilized by EF loops to coordinate ions that have a smaller ionic radius than calcium (Grabarek, 2011). For example, in calbindin D9k the C-terminal EF loop utilizes canonical pentagonal bipyramidal coordination when bound to Ca^{2+} (Svensson *et al.*, 1992) but octahedral coordination when bound to Mg^{2+} (Andersson *et al.*, 1997). The octahedral coordination allows the EF loop to achieve optimum coordination angles with the smaller ion (Grabarek, 2011). In all cases of octahedral coordination desc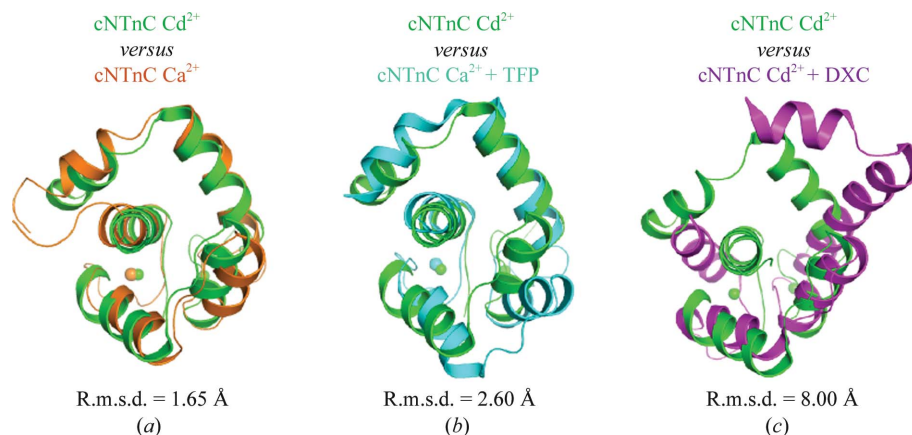ribed above, including the structure presented here, a common feature is observed: the bidentate ligand at position 12 ($-Z$), which is usually a glutamate, is too distant from the coordination sphere and is therefore replaced by a water molecule or an acetate ion. Interestingly, a metalloprotease that does not contain an EF-hand motif has been observed to bind Cd^{2+} (replacing the native Zn^{2+} ion) *via* a 'distorted' octahedral geometry using waters and histidine side chains as ligands (Huang *et al.*, 2002).

3.6. Cys35 plays an important role in coordinating the Cd^{2+} in EF1

Although not evolved to bind Ca^{2+} under physiological conditions, the vestigial EF1 site in the cNTnC structure

Figure 5
Superposition of the Cd^{2+}-bound cNTnC structure with other cNTnC structures. All structures are presented as ribbon diagrams. The Cd^{2+}-bound cNTnC is in green and is superimposed with (a) a representative chain from the NMR structure of Ca^{2+}-bound cNTnC (orange, PDB entry 1ap4, Spyracopoulos *et al.*, 1997), (b) chain A of Ca^{2+}-bound cNTnC in complex with TFP (cyan, PDB entry 1wrk, S. Takeda, T. Igarashi, Y. Oishi & H. Mori, unpublished work) and (c) chain A of Cd^{2+}-bound cNTnC in complex with DXC (magenta, PDB entry 3rv5; Li *et al.*, 2011). R.m.s.d.s are shown below each superposition.
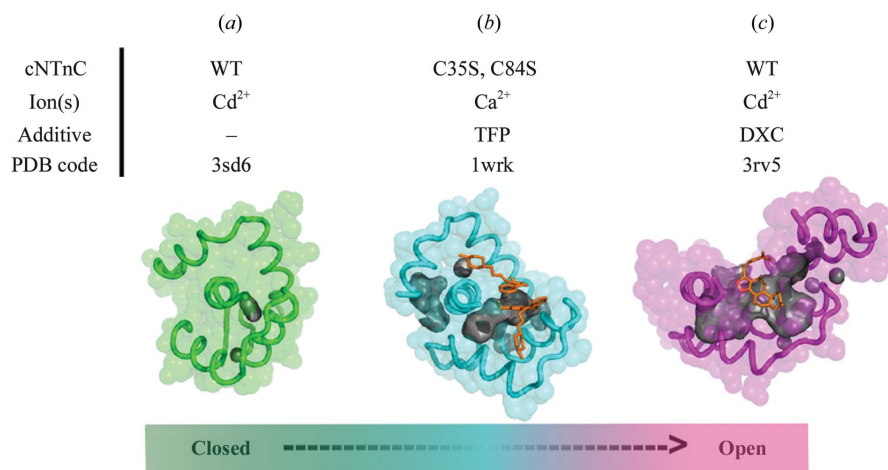

Figure 6
Crystal structures of cNTnC placed on a 'closed-to-open' scale. (a) Cd^{2+}-bound cNTnC (green), (b) Ca^{2+}-bound cNTnC in complex with TFP (trifluoroperazine, orange; protein, cyan) and (c) Cd^{2+}-bound cNTnC in complex with DXC (deoxycholic acid, orange; protein, magenta) are displayed as ribbons with semitransparent surfaces. Dark grey blobs represent the void area of the central hydrophobic cavity on the protein surface in each cNTnC protein.

shown here coordinates a Cd^{2+} ion with full occupancy and strong electron density that clearly reveals the coordination geometry (Fig. 7a). While the similarity in the ionic radius of Cd^{2+} and Ca^{2+} allows Cd^{2+} to fit in the EF1 loop, the presence of cysteine in the EF1 loop is proposed to play a major role in coordinating Cd^{2+} at this vestigial site. Comparing EF1 in cNTnC with skeletal troponin C, which has a functional EF1 that coordinates Ca^{2+}, the unique presence of cysteine (Cys35) in the vestigial EF1 of cNTnC makes this loop more adaptable for Cd^{2+} binding. The cysteine S^{γ} atom tends to form a thiolate bond with the soft metal Cd^{2+} rather than the hard metal Ca^{2+} (Jalilehvand et al., 2009). Although the amino-acid sequence of EF1 makes the classical pentagonal bipyramidal coordination of Ca^{2+} difficult, the presence of cysteine and the flexibility of Cd^{2+} coordination in the protein makes the EF1 loop a great niche for Cd^{2+}, as shown in the structure presented here. Similar examples are cysteine-rich proteins such as metallothioneins (MTs), which can actively remove Cd^{2+} in vivo by thiolate coordination with cysteine residues (Boulanger et al., 1982; Melis et al., 1983).

The cysteine in the EF1 loop, Cys35, also participates in coordinating Cd^{2+} intermolecularly. This connection between cysteine of one molecule and Cd^{2+} from the neighbouring molecule plays an important role in crystal packing. Parallel crystallization trials with identical experimental conditions were set up for both WT and C35S cNTnC. While WT cNTnC crystallized and generated the high-resolution structure, C35S cNTnC yielded no crystals.

3.7. Intermolecular Cd^{2+} promotes crystallization

Cd^{2+} ions are bound in both the EF1 and EF2 loops (Fig. 2a). As well as these two Cd^{2+} ions, five other Cd^{2+} and two Ca^{2+} ions are found in each asymmetric unit. These ions are positioned between the protein and its symmetry-related molecules. Crystallization does not occur under these conditions with less than 20 mM CdSO$_4$. This high concentration of Cd^{2+} and the large number of Cd^{2+} ions coordinated between neighbouring protein molecules suggest that these ions play an important role in crystal packing. A similar situation has been shown for leucine/isoleucine/valine-binding protein (LIVBP; Trakhanov & Quiocho, 1995). Various divalent ions were screened to optimize crystallization conditions for LIVBP, and Cd^{2+} was found to generate the most ordered crystals with the highest diffraction (Trakhanov & Quiocho,

1995). Addition of Cd^{2+} also improved the crystal morphology of histidine-binding protein (Trakhanov et al., 1998). In all of the cases mentioned above, the Cd^{2+} concentration needs to reach a certain level for crystallization to occur (e.g. 1 mM for LIVBP and 20 mM for cNTnC). The concentration needed for crystallization correlates with the abundance and distribution of negatively charged residues on the protein surface (Trakhanov et al., 1998). Since 25.9% of cNTnC residues are acidic, this protein is a good candidate for utilizing Cd^{2+} to promoting crystallization.

Fig. 8 shows all of the intermolecular Cd^{2+} ions in cNTnC (Fig. 8a) and cNTnC bound to DXC (Fig. 8b). The Cd^{2+} ions are coordinated in various arrangements (e.g. tetrahedral, trigonal bipyramidal and octahedral) intermolecularly in both structures. The majority of the coordinating residues are negatively charged glutamates and aspartates. The only residue that is conserved between the two structures in coordinating intermolecular Cd^{2+} is Cys35. This again stresses the important relationship between Cys35 and Cd^{2+} in this structure, as discussed in the previous section. Table 2 summarizes the coordination of intermolecular Cd^{2+} in the two cNTnC structures shown in Fig. 8.
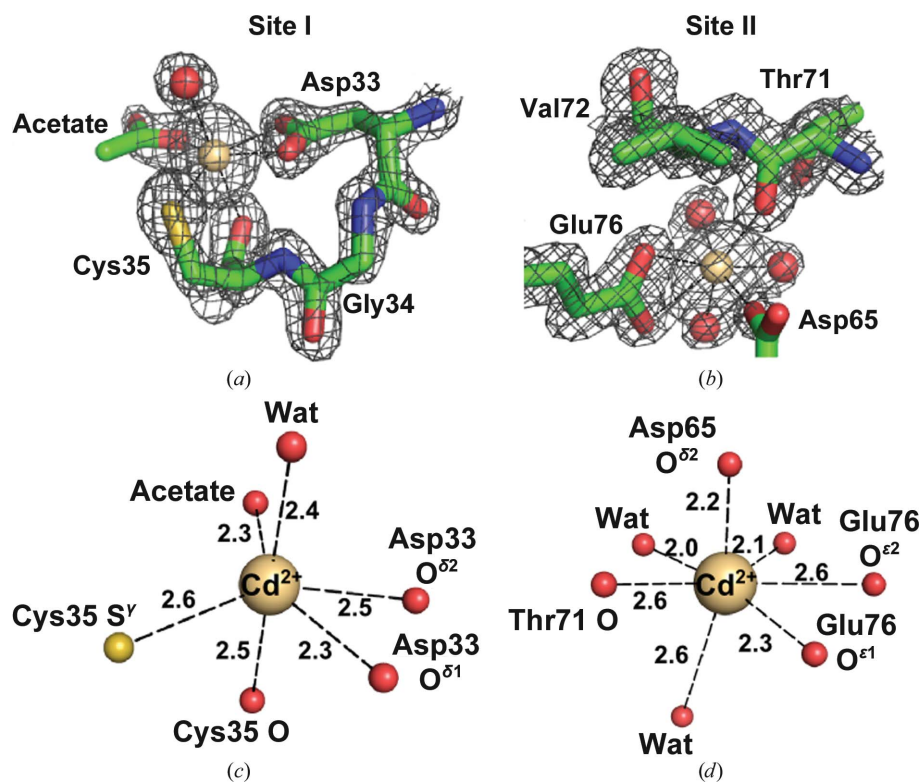

Figure 7
Electron density and coordination geometry of Cd^{2+} in the EF1 and EF2 loops of cNTnC. (a) The electron density for residues within proximity of the Cd^{2+} ion at EF1. (b) The electron density for residues within proximity of the Cd^{2+} ion at EF2. The residues are rendered as sticks (carbon, green; nitrogen, blue; oxygen, red; sulfur, yellow). The Cd^{2+} ion and water molecules are represented by light orange and red spheres, respectively. The σ level of the $2F_o - F_c$ electron density is 1.5σ in (a) and 1.0σ in (b). (c) The atoms involved in Cd^{2+} coordination and their atomic distances are shown for EF1. (d) The atoms involved in Cd^{2+} coordination and their atomic distances are shown for EF2. The Cd^{2+} ions are depicted as light orange spheres. Atomic distances are indicated in Å. The coordinating atoms are shown as small spheres (oxygen, red, sulfur, yellow).

Table 2
Coordination of intermolecular Cd^{2+} in two cNTnC structures.

	Open conformation (PDB entry 3rv5)		Closed conformation (PDB entry 3sd6)	
Asymmetric unit contents				
Protein molecules	4		1	
Total Cd^{2+}	21		7	
Cd^{2+} in EF hands	8		2	
Cd^{2+} coordinated intermolecularly	6		5	
Intermolecular Cd	Cd103A	Cys35A (S^γ)	Cd101, occupancy = 1.0	Phe27 (O)
		HOH115A, 118A, 119A		Glu40 ($O^{\varepsilon1}$, $O^{\varepsilon2}$)
		Glu15A ($O^{\varepsilon2}$) [Symm]		HOH125, 145
		Glu19A ($O^{\varepsilon1}$, $O^{\varepsilon2}$) [Symm]		Glu63 ($O^{\varepsilon1}$, $O^{\varepsilon2}$) [Symm]
	Cd105B	Glu32B ($O^{\varepsilon1}$, $O^{\varepsilon2}$)	Cd102, occupancy = 1.0	Glu56 ($O^{\varepsilon1}$, $O^{\varepsilon2}$)
		HOH142B, 148B		Cys84 (S^γ)
		Glu15C ($O^{\varepsilon2}$)		Asp87 ($O^{\delta2}$)
		HOH138C		Ser89 (O, OXT) [Symm]
	Cd106B	Glu59B ($O^{\varepsilon1}$, $O^{\varepsilon2}$)	Cd103, occupancy = 1.0	Gln50 ($O^{\varepsilon1}$)
		HOH133B, 134B, 135B		Cys84 (S^γ, O)
		DXC92A (O3, O4) [Symm]		Asp87 ($O^{\delta1}$)
	Cd107B	Asp62B ($O^{\delta2}$)		Asp88 ($O^{\delta1}$, $O^{\delta2}$) [Symm]
		Glu14A ($O^{\varepsilon1}$, $O^{\varepsilon2}$) [Symm]		Ser89 (O) [Symm]
	Cd105C	Glu59C ($O^{\varepsilon1}$, $O^{\varepsilon2}$)	Cd105, occupancy = 1.0	Glu66 ($O^{\varepsilon1}$, $O^{\varepsilon2}$)
		Glu10D ($O^{\varepsilon2}$) [Symm]		Asp73 ($O^{\delta1}$, $O^{\delta2}$)
		DXC92D (O4) [Symm]		Asp75 ($O^{\delta1}$, $O^{\delta2}$)
	Cd103D	Cys35D (S^γ)		Cys35 (S^γ) [Symm]
		HOH128D	Cd106, occupancy = 0.6	Glu59 ($O^{\varepsilon1}$, $O^{\varepsilon2}$)
		Glu15D ($O^{\varepsilon2}$) [Symm]		HOH131, 132, 133, 146
		Glu19D ($O^{\varepsilon1}$, $O^{\varepsilon2}$) [Symm]		Met1 (O) [Symm]
Other Cd	Cd104A	Asp73A ($O^{\delta1}$, $O^{\delta2}$)		
		Asp75A ($O^{\delta1}$, $O^{\delta2}$)		
		HOH120A, 127A, 132A		
	Cd105A	Glu66A ($O^{\varepsilon1}$, $O^{\varepsilon2}$)		
		HOH140A		
		HOH123C, 138C		
	Cd103B	Cys35B (S^γ)		
		HOH119B, 144B, 146B, 147B, 150B		
	Cd104B	Asp73B ($O^{\delta1}$, $O^{\delta2}$)		
		Asp75B ($O^{\delta1}$, $O^{\delta2}$)		
		HOH113B, 114B, 115B, 138B		
	Cd103C	Asp33C ($O^{\delta1}$)		
		Cys35C (S^γ)		
		HOH111C, 116C, 133C, 143C		
	Cd104C	Asp73C ($O^{\delta1}$, $O^{\delta2}$)		
		Asp75C ($O^{\delta1}$, O^{δ}2)		
		HOH113C, 119C, 130C		
	Cd104D	Asp73D ($O^{\delta1}$, $O^{\delta2}$)		
		Asp75D ($O^{\delta1}$, $O^{\delta2}$)		
		HOH118D, 120D		

3.8. EF2 coordinates Cd^{2+} in a canonical pentagonal bipyramidal geometry using only three residues; the occupancy of Cd^{2+} in EF1 and EF2 supports the Ca^{2+}-binding nature of the EF-hand motif

Our structure shows that EF2 coordinates Cd^{2+} in a canonically pentagonal bipyramidal geometry (Fig. 7b). Four of the ligands come from Asp65 $O^{\delta2}$ (X), Thr71 O ($-Y$) and Glu76 $O^{\varepsilon1}$/$O^{\varepsilon2}$ ($-Z$) and three others from water molecules ($-X$, Y and Z) (Fig. 7d). Since two of the conserved residues, Asp67 (Y) and Ser69 (Z), are not observed in the electron density (they are presumably in a dynamic state; see §3.2), water molecules substitute for the disordered ligands. To our knowledge, this is the first time such an ion coordination has been observed in cNTnC or any other EF-hand protein. This

reveals tremendous flexibility in the ion-coordination repertoire of this protein.

The EF-hand motif is normally present in proteins for the purpose of Ca^{2+} binding. The Ca^{2+}-binding loop in the EF-hand motif has evolved to be very specific in sequence and spatial arrangement for accommodation of the Ca^{2+} ion. The coordinating ligands come together to coordinate Ca^{2+} with a pentagonal bipyramidal geometry. Any ion with a larger or smaller ionic radius would not fit as well in the EF loop.

In contrast to the full occupancy and sharp electron density of Cd^{2+} coordination in EF1, the occupancy of Cd^{2+} in EF2 is partial (0.5 in WT cNTnC; 0.6 in L29Q and NIQD cNTnC) and the electron density of three EF2-loop residues was missing. The B factors of Cd^{2+} in EF2 in all of the structures presented here are higher than those of Cd^{2+} in their corre-

sponding EF1 loops. This is the first structural evidence for a disordered region in the EF2 loop of troponin C. For the functional EF2, which is designed for Ca^{2+} binding with its conserved coordination residues, the presence of Cd^{2+} is likely to destabilize and disorder this region, which results in the missing electron densities for the three loop residues.

3.9. Cd^{2+} coordination in EF-hand proteins

Cadmium bound to EF-hand motif-containing proteins other than cNTnC have previously been structurally investigated (Li *et al.*, 2011; Rao *et al.*, 1996; Leinala *et al.*, 2003; Swain *et al.*, 1989). Fig. 9 compares the ion-coordinating
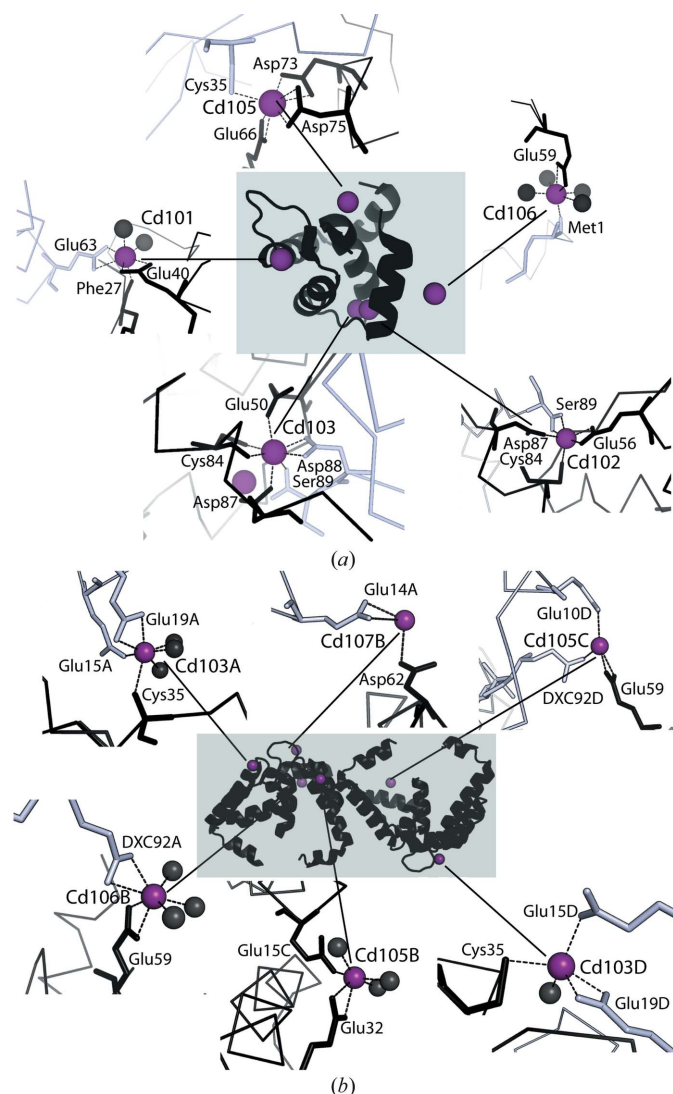
Figure 8
Intermolecular Cd^{2+} coordination in cNTnC and cNTnC complexed with DXC. Intermolecular Cd^{2+} ions (purple spheres) and their spatial arrangement around both (*a*) cNTnC and (*b*) cNTnC complexed with DXC (deoxycholic acid; protein rendered as a black cartoon) are shown in the shaded area. The coordination details of each intermolecular Cd^{2+} ion are also presented around the shaded area. The protein chain and its neighbouring symmetry-related molecule that coordinate the Cd^{2+} ion are shown as black and white Cα traces, respectively. Coordinating residues are labelled and rendered in sticks in the corresponding chain colours. Grey spheres are water molecules that coordinate Cd^{2+}.

Table 3
Cd^{2+} bound to EF-hand motif-containing proteins: distance (Å) between ligand atom and Cd^{2+}.

	EF1		EF2	
Parvalbumin (PDB entry 1cdp; Swain *et al.*, 1989)				
X	Asp51 $O^{\delta 1}$	2.1	Asp90 $O^{\delta 2}$	2.3
Y	Asp53 $O^{\delta 1}$	2.4	Asp92 $O^{\delta 1}$	2.4
Z	Ser55 O^{γ}	2.6	Asp94 $O^{\delta 1}$	2.2
$-Y$	Phe57 O	2.3	Lys96 O	2.3
$-X$	Glu59 $O^{\varepsilon 1}$	2.3	HOH116 O	2.4
$-Z$	Glu62 $O^{\varepsilon 1}$	2.8	Glu101 $O^{\varepsilon 1}$	2.3
	Glu62 $O^{\varepsilon 2}$	2.4	Glu101 $O^{\varepsilon 2}$	2.7
Calpain (PDB entry 1np8; Leinala *et al.*, 2003)				
X	Ala25 O	2.2	Asp68 $O^{\delta 1}$	2.3
Y	HOH726 O	2.5	Asp70 $O^{\delta 1}$	2.3
Z	Asp28 $O^{\delta 1}$	2.2	Thr72 O^{γ}	2.5
$-Y$	Glu30 O	2.4	Lys74 O	2.3
$-X$	HOH772 O	2.3	HOH778 O	2.4
$-Z$	Glu35 $O^{\varepsilon 1}$	2.4	Glu79 $O^{\varepsilon 1}$	2.1
	Glu35 $O^{\varepsilon 2}$	2.4	Glu79 $O^{\varepsilon 2}$	2.9
Cardiac troponin C with DXC (PDB entry 3rv5; Li *et al.*, 2011)				
X	Gly30 O	2.2	Asp65 $O^{\delta 2}$	2.1
Y	Asp33 $O^{\delta 1}$	2.4	Asp67 $O^{\delta 1}$	2.3
Z	Asp33 $O^{\delta 2}$	2.1	Ser69 O^{γ}	2.3
$-Y$	Cys35 O	2.5	Thr71 O	2.4
$-X$	Cys35 S	2.5	HOH110 O	2.3
$-Z$	Glu40 $O^{\varepsilon 1}$	2.4	Glu76 $O^{\varepsilon 1}$	2.3
	Glu40 $O^{\varepsilon 2}$	2.6	Glu76 $O^{\varepsilon 2}$	2.6
Skeletal troponin C (PDB entry 1ncx; Rao *et al.*, 1996)				
X	Asp106 $O^{\delta 1}$	2.0	Asp142 $O^{\delta 1}$	2.1
Y	Asn108 $O^{\delta 1}$	2.3	Asn144 $O^{\delta 1}$	2.4
Z	Asp110 $O^{\delta 1}$	2.3	Asp146 $O^{\delta 1}$	2.3
$-Y$	Phe112 O	2.3	Arg148 O	2.3
$-X$	HOH176 O	2.2	HOH209 O	2.3
$-Z$	Glu117 $O^{\varepsilon 1}$	2.5	Glu153 $O^{\varepsilon 1}$	2.4
	Glu117 $O^{\varepsilon 2}$	2.5	Glu153 $O^{\varepsilon 2}$	2.6
Cardiac troponin C (PDB entry 3sd6; this work)				
X	Cys35 O	2.5	Asp65 $O^{\delta 2}$	2.2
Y	Asp33 $O^{\delta 2}$	2.5	HOH147 O	2.1
Z	Asp33 $O^{\delta 1}$	2.3	HOH148 O	2.0
$-Y$	Cys35 S^{γ}	2.6	Thr71 O	2.6
$-X$	HOH97 O	2.4	HOH151 O	2.6
$-Z$	ACT90 OXT	2.3	Glu76 $O^{\varepsilon 1}$	2.3
			Glu76 $O^{\varepsilon 2}$	2.6

residues in EF loops from five Cd^{2+}-bound EF-hand structures. These structures are of parvalbumin (Swain *et al.*, 1989), calpain (Leinala *et al.*, 2003), cardiac troponin C in complex with DXC (Li *et al.*, 2011), skeletal troponin C (Rao *et al.*, 1996) and cardiac troponin C. The detailed spatial orientations of the coordinating ligands and atomic distances are listed in Table 3. All of these proteins are well known Ca^{2+}-binding proteins. Except for EF1 in our cardiac troponin C structure, all of the EF loops coordinate Cd^{2+} in the canonical pentagonal bipyramidal geometry, as shown in Fig. 9.

Canonically, five EF-loop residues at positions 1, 3, 5, 7 and 12 contribute coordinating ligands. In EF1 of the structure presented here, only two residues, Asp33 and Cys35 (positions 5 and 7), contribute to the ion coordination. As mentioned, the EF1 loop in cNTnC does not normally bind ions (vestigial site); however, the structure presented here shows that EF1 manages to coordinate Cd^{2+} by changing the loop conformation. This also causes the side chain of the residue at position 12, glutamate, to point away from the coordination site so that it is not available for coordinating the Cd^{2+} in the canonical fashion. This feature can be observed by comparing the EF1
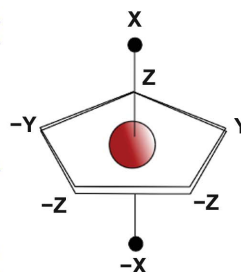
Cd²⁺-bound EF-hand structures

Figure 9
The residues used to coordinate Cd^{2+} in EF-hand protein structures. EF-hand loop sequences of parvalbumin (PDB entry 1cdp; Swain *et al.*, 1989), calpain (PDB entry 1np8; Leinala *et al.*, 2003), cardiac troponin C complexed with DXC (PDB entry 3rv5; Li *et al.*, 2011), skeletal troponin C (PDB entry 1ncx; Rao *et al.*, 1996) and cardiac troponin C (PDB entry 3sd6; this work) are shown. Spatial orientation assignments of the coordinating ligands are labelled either above or below the residues. The canonical pentagonal bipyramidal geometry labels are schematically shown for reference.

coordination (listed in Table 3) between cNTnC with bound DXC and the cNTnC structure presented here.

EF2 in cNTnC–DXC and EF2 in the cNTnC structure presented here both coordinate Cd^{2+} in the canonical fashion. The two EF loops in skeletal troponin C also coordinate Cd^{2+} canonically (Rao *et al.*, 1996), leading to the conclusion that Cd^{2+} ions are able to substitute for Ca^{2+} ions in EF hands in a canonical fashion. Indeed, functional data show that Cd^{2+} can activate skeletal troponin C (in which site I is functional) by substituting for Ca^{2+} (Chao *et al.*, 1990).

By comparing the EF-loop sequences of the five proteins in Fig. 9, it can be seen that cardiac troponin C is the only one with cysteine as a coordination residue, bearing in mind that the cysteine is coordinating a Cd^{2+} ion in a vestigial ion-binding site, so its significance is not clear in a physiological sense. To our knowledge, there is no other example of an EF-hand protein in which cysteine serves as an ion-coordinating ligand. Interestingly, this is not the case in non-EF-hand proteins.

3.10. Cd²⁺ coordination in non-EF-hand proteins

Cadmium, with a filled d^{10} orbital shell, can take on a number of different coordination geometries. Examination of non-EF-hand proteins in complex with Cd^{2+} reveals that Cd^{2+} is most often coordinated in either tetrahedral or trigonal bipyramidal geometries, with histidine and cysteine residues most frequently involved in coordinating the Cd^{2+} ion. For example, in cadmium carbonic anhydrase (CDCA; Xu *et al.*, 2008) and horse liver alcohol dehydrogenase (Meijers *et al.*,

2001), Cd^{2+} is coordinated by two cysteines, one histidine and two water molecules in a trigonal bipyramidal geometry. Histidines are normally involved in tetrahedral coordination (Benning *et al.*, 2001; Ferraroni *et al.*, 1999), and in one case, octahedral coordination (Huang *et al.*, 2002). The ionic radius of Cd^{2+} is similar to that of Ca^{2+}, and this similarity in size and charge make the two ions competitors for the same protein ion-binding sites (Mastrángelo *et al.*, 2011; Adiele *et al.*, 2012). As shown in the examples above, Cd^{2+} appears to be more flexible in its coordination number and geometry than Ca^{2+}. Cd^{2+} is also able to replace Zn^{2+} ions in many proteins (Xu *et al.*, 2008; Meijers *et al.*, 2001).

3.11. Refolded cNTnC

The 1.6 Å resolution structure of *in vitro* refolded WT cNTnC rendered the same conformation as the WT cNTnC (r.m.s.d. = 0.057 Å), which was natively folded within the cytoplasm of the expression host. This suggests that refolding of cNTnC does not alter the fold of the protein.

The troponin complex has been studied for decades and troponin C has been purified in various ways, including direct purification from muscle tissue and expression using *E. coli*. Regardless of the initial source of the protein, the majority of the previous studies have used refolded troponin C. The WT, L29Q and NIQD cNTnC structures presented here were expressed in *E. coli* and purified under nondenaturing conditions. To investigate any possible structural difference between refolded and non-refolded cNTnC, the refolded cNTnC was crystallized and the same crystal form was generated as for the non-refolded WT cNTnC. Therefore, regardless of the refolding status of cNTnC the protein renders the same conformation, as indicated by the presented crystal structures.

3.12. Cd²⁺ in the cNTnC vestigial site, a potential means of cardiac toxicity

Cadmium is a soft metal that can form a covalent bond with the thiol S atom of cysteine (Dokmanić *et al.*, 2008). Therefore, it is possible that Cd^{2+} cannot dissociate from the EF1 loop once it has been coordinated. Although EF1 is a vestigial site in cNTnC, it has previously been shown to have a functional effect on the protein (Gillis *et al.*, 2005, 2007). Cadmium, which is not normally present in more than trace amounts in mammals, is a toxic metal and can disrupt physiological function (Houston, 2007; Peters *et al.*, 2010). For example, intake of Cd^{2+} in rats has been shown to cause irregular cardiac function (Kopp *et al.*, 1983). The formation of a

potential covalent cadmium–sulfur bond leading to the inability of Cd^{2+} to dissociate from EF1 of cNTnC could suggest a potential contributor to the toxicity of cadmium *via* cardiac dysfunction.

References

Adams, P. D. *et al.* (2010). *Acta Cryst.* D**66**, 213–221.
Adiele, R. C., Stevens, D. & Kamunde, C. (2012). *Toxicol. In Vitro*, **26**, 164–173.
Andersson, M., Malmendal, A., Linse, S., Ivarsson, I., Forsén, S. & Svensson, L. A. (1997). *Protein Sci.* **6**, 1139–1147.
Benning, M. M., Shim, H., Raushel, F. M. & Holden, H. M. (2001). *Biochemistry*, **40**, 2712–2722.
Boulanger, Y., Armitage, I. M., Miklossy, K. A. & Winge, D. R. (1982). *J. Biol. Chem.* **257**, 13717–13719.
Chao, S., Bu, C.-H. & Cheung, W. Y. (1990). *Arch. Toxicol.* **64**, 490–496.
DeLano, W. L. (2002). *PyMOL*. http://www.pymol.org.
Dokmanić, I., Šikić, M. & Tomić, S. (2008). *Acta Cryst.* D**64**, 257–263.
Eerd, J. P. van & Takahashi, K. (1975). *Biochem. Biophys. Res. Commun.* **64**, 122–127.
Emsley, P. & Cowtan, K. (2004). *Acta Cryst.* D**60**, 2126–2132.
Endoh, M. (2007). *Br. J. Pharmacol.* **150**, 826–828.
Farah, C. S. & Reinach, F. C. (1995). *FASEB J.* **9**, 755–767.
Ferraroni, M., Rypniewski, W., Wilson, K. S., Viezzoli, M. S., Banci, L., Bertini, I. & Mangani, S. (1999). *J. Mol. Biol.* **288**, 413–426.
Forsén, S., Thulin, E. & Lilja, H. (1979). *FEBS Lett.* **104**, 123–126.
Genicot, S., Rentier-Delrue, F., Edwards, D., VanBeeumen, J. & Gerday, C. (1996). *Biochim. Biophys. Acta*, **1298**, 45–57.
Gifford, J. L., Walsh, M. P. & Vogel, H. J. (2007). *Biochem. J.* **405**, 199–221.
Gillis, T. E., Liang, B., Chung, F. & Tibbits, G. F. (2005). *Physiol. Genomics*, **22**, 1–7.
Gillis, T. E., Marshall, C. R. & Tibbits, G. F. (2007). *Physiol. Genomics*, **32**, 16–27.
Gordon, A. M., Homsher, E. & Regnier, M. (2000). *Physiol. Rev.* **80**, 853–924.
Grabarek, Z. (2006). *J. Mol. Biol.* **359**, 509–525.
Grabarek, Z. (2011). *Biochim. Biophys. Acta*, **1813**, 913–921.
Hoffmann, B., Schmidt-Traub, H., Perrot, A., Osterziel, K. J. & Gessner, R. (2001). *Hum. Mutat.* **17**, 524.
Hofmann, A. F. (1999). *Arch. Intern. Med.* **159**, 2647–2658.
Houston, M. C. (2007). *Altern. Ther. Health Med.* **13**, S128–S133.
Huang, K.-F., Chiou, S.-H., Ko, T.-P., Yuann, J.-M. & Wang, A. H.-J. (2002). *Acta Cryst.* D**58**, 1118–1128.
Jalilehvand, F., Leung, B. O. & Mah, V. (2009). *Inorg. Chem.* **48**, 5758–5771.
Jia, J., Tarabykina, S., Hansen, C., Berchtold, M. & Cygler, M. (2001). *Structure*, **9**, 267–275.
Kass, D. A. & Solaro, R. J. (2006). *Circulation*, **113**, 305–315.
Kopp, S. J., Perry, H. M., Perry, E. F. & Erlanger, M. (1983). *Toxicol. Appl. Pharmacol.* **69**, 149–160.
Kretsinger, R. H. & Nockolds, C. E. (1973). *J. Biol. Chem.* **248**, 3313–3326.
Leinala, E. K., Arthur, J. S., Grochulski, P., Davies, P. L., Elce, J. S. & Jia, Z. (2003). *Proteins*, **53**, 649–655.
Li, A. Y., Lee, J., Borek, D., Otwinowski, Z., Tibbits, G. F. & Paetzel, M. (2011). *J. Mol. Biol.* **413**, 699–711.
Li, M. X., Gagné, S. M., Spyracopoulos, L., Kloks, C. P. A. M., Audette, G., Chandra, M., Solaro, R. J., Smillie, L. B. & Sykes, B. D. (1997). *Biochemistry*, **36**, 12519–12525.
Li, M. X., Spyracopoulos, L. & Sykes, B. D. (1999). *Biochemistry*, **38**, 8289–8298.
Liang, B., Chung, F., Qu, Y., Pavlov, D., Gillis, T. E., Tikunova, S. B., Davis, J. P. & Tibbits, G. F. (2008). *Physiol. Genomics*, **33**, 257–266.
Mastrángelo, M., Dos Santos Afonso, M. & Ferrari, L. (2011). *Ecotoxicology*, **20**, 1225–1232.
McCoy, A. J., Grosse-Kunstleve, R. W., Adams, P. D., Winn, M. D., Storoni, L. C. & Read, R. J. (2007). *J. Appl. Cryst.* **40**, 658–674.
Meijers, R., Morris, R. J., Adolph, H. W., Merli, A., Lamzin, V. S. & Cedergren-Zeppezauer, E. S. (2001). *J. Biol. Chem.* **276**, 9316–9321.
Melis, K. A., Carter, D. C., Stout, C. D. & Winge, D. R. (1983). *J. Biol. Chem.* **258**, 6255–6257.
Murshudov, G. N., Skubák, P., Lebedev, A. A., Pannu, N. S., Steiner, R. A., Nicholls, R. A., Winn, M. D., Long, F. & Vagin, A. A. (2011). *Acta Cryst.* D**67**, 355–367.
Otwinowski, Z. & Minor, W. (1997). *Methods Enzymol.* **276**, 307–326.
Pape, T. & Schneider, T. R. (2004). *J. Appl. Cryst.* **37**, 843–844.
Peters, J. L., Perlstein, T. S., Perry, M. J., McNeely, E. & Weuve, J. (2010). *Environ. Res.* **110**, 199–206.
Rao, S. T., Satyshur, K. A., Greaser, M. L. & Sundaralingam, M. (1996). *Acta Cryst.* D**52**, 916–922.
Robertson, I. M., Sun, Y.-B., Li, M. X. & Sykes, B. D. (2010). *J. Mol. Cell. Cardiol.* **49**, 1031–1041.
Smalås, A. O., Heimstad, E. S., Hordvik, A., Willassen, N. P. & Male, R. (1994). *Proteins*, **20**, 149–166.
Spyracopoulos, L., Li, M. X., Sia, S. K., Gagné, S. M., Chandra, M., Solaro, R. J. & Sykes, B. D. (1997). *Biochemistry*, **36**, 12138–12146.
Strynadka, N. C. & James, M. N. G. (1989). *Annu. Rev. Biochem.* **58**, 951–998.
Svensson, L. A., Thulin, E. & Forsén, S. (1992). *J. Mol. Biol.* **223**, 601–606.
Swain, A. L., Kretsinger, R. H. & Amma, E. L. (1989). *J. Biol. Chem.* **264**, 16620–16628.
Trakhanov, S., Kreimer, D. I., Parkin, S., Ames, G. F. & Rupp, B. (1998). *Protein Sci.* **7**, 600–604.
Trakhanov, S. & Quiocho, F. A. (1995). *Protein Sci.* **4**, 1914–1919.
Vagin, A. & Teplyakov, A. (2010). *Acta Cryst.* D**66**, 22–25.
Walker, J. M. (2005). Editor. *The Proteomics Protocols Handbook.* Totowa: Humana Press.
Wang, X., Li, M. X. & Sykes, B. D. (2002). *J. Biol. Chem.* **277**, 31124–31133.
Wang, L., Seidman, J. G. & Seidman, C. E. (2010). *Ann. Intern. Med.* **152**, 513–520.
Winn, M. D. *et al.* (2011). *Acta Cryst.* D**67**, 235–242.
Xu, Y., Feng, L., Jeffrey, P. D., Shi, Y. & Morel, F. M. (2008). *Nature (London)*, **452**, 56–61.